ACS OMEGA

Open Access

http://pubs.acs.org/journal/acsodf

Article

Effect of Gentamicin Sulfate and Polymeric Polyethylene Glycol Coating on the Degradation and Cytotoxicity of Iron-Based Biomaterials

Martina Petráková, Radka Gorejová, Jana Shepa, Ján Macko, Miriam Kupková, Matej Mičušík, Matej Baláž, Vanda Hajdučková, Patrícia Hudecová, Martin Kožár, Barbora Šišková, Petr Sáha, and Renáta Oriňaková*

Cite This: *ACS Omega* 2024, 9, 27113−27126

Read Online

ACCESS | Metrics & More | Article Recommendations

ABSTRACT: The work is focused on the degradation, cytotoxicity, and antibacterial properties, of iron-based biomaterials with a bioactive coating layer. The foam and the compact iron samples were coated with a polyethylene glycol (PEG) polymer layer without and with gentamicin sulfate (PEG + Ge). The corrosion properties of coated and uncoated samples were studied using the degradation testing in Hanks' solution at 37 °C. The electrochemical and static immersion corrosion tests revealed that the PEG-coated samples corroded faster than samples with the bioactive PEG + Ge coating and uncoated samples. The foam samples corroded faster compared with the compact samples. To determine the cytotoxicity, cell viability was monitored in the presence of porous foam and compact iron samples. The antibacterial activity of the samples with PEG and PEG + Ge against *Escherichia coli* CCM 3954 and *Staphylococcus aureus* CCM 4223 strains was also tested. Tested PEG + Ge samples showed significant antibacterial activity against both bacterial strains. Therefore, the biodegradable iron-based materials with a bioactive coating could be a suitable successor to the metal materials studied thus far as well as the materials used in the field of medicine.

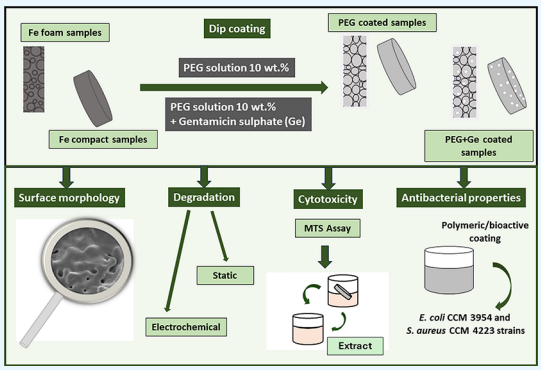

1. INTRODUCTION

There is a long-term growing demand for orthopedic implants in the world, mainly due to the increased number of fractures and injuries, especially in the elderly population. These injuries significantly affect the quality of life of patients; therefore, bone implants have become a sought-after group of implants.[1,2] Metals play an important role in the human body. In the form of implants, metals are used, for example, in bone joint replacements and dental implants. Most metal implants find application in orthopedic surgery due to their advantages, such as higher tensile strength and durability compared to ceramics and polymers. Metals, such as stainless steel, Co−Cr alloys, or titanium and its alloys, are still used in biomedical permanent implants.[3−5]

Biodegradable materials have become a trend in recent years. Their biggest advantage is controlled resorption directly in the patient's body. Metallic biodegradable biomaterials have good mechanical properties, but they are made of metals that can be released in a certain amount due to the corrosive environment of body fluids. Therefore, in addition to the possible toxicity of the material, the potential toxicity of its degradation products must also be considered. These properties affect the living system in which they are implanted and can lead to deterioration of the implant's properties, resulting in damage to the implant itself and consequently to a reduction in its biocompatibility.[6−9]

Iron as a biomaterial is compatible with human physiology, has a similar density to human bone, as well as good mechanical compatibility.[10] This work focuses on iron porous as well as compact materials because, despite the indisputable advantages of porous materials, some properties of compact iron can be used in load-bearing applications. In the same way, the use of compact materials compared to foams is advantageous, for example, in some tests as reference materials, for example, from the point of view of biocompatibility testing. Compact iron exhibits a Young's modulus of 210 GPa. However, Young's modulus is in the range of 10−20 GPa for

Received: January 31, 2024
Revised: May 17, 2024
Accepted: May 24, 2024
Published: June 12, 2024

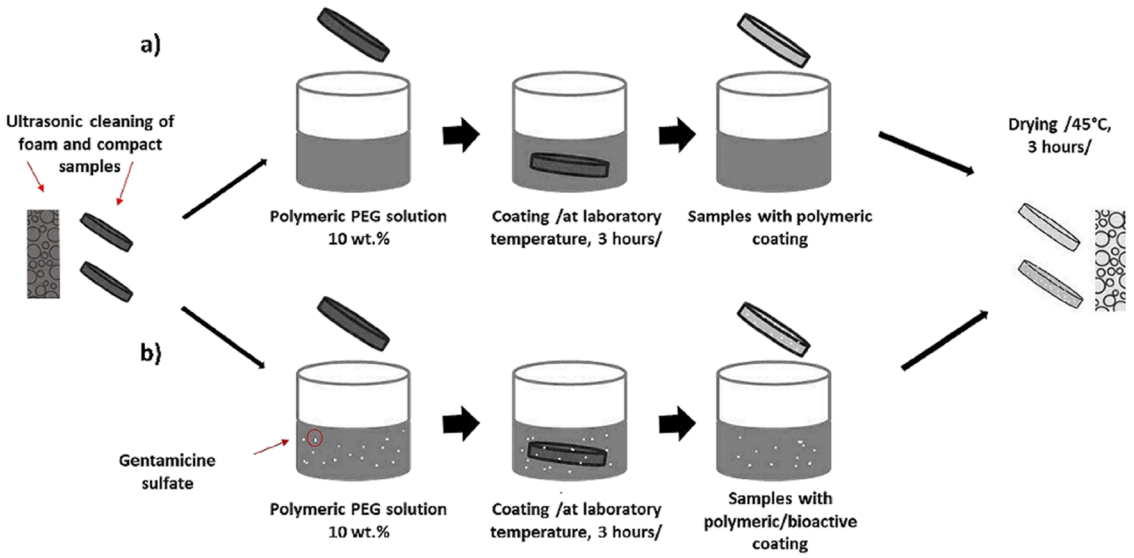

Figure 1. (a) Polymeric and (b) bioactive coating deposition scheme.

cancellous bone and 3×10^{-4}–3×10^{-3} GPa for trabecular bone. The use of compact iron materials in the form of implants can result in stress shielding mainly due to the different stiffness of the implant and the bone, which is precisely what the production and use of porous iron materials are trying to prevent. Porous iron-based materials with porosity in the range of 45.6–86.9% exhibit a compressive modulus of elasticity in the range of 218–845 MPa, which is close to the values of trabecular bone. The size and mutual connectivity of the pores represent the key factors that influence the biological and mechanical properties of porous materials.[11,12]

The porous structure of degradable materials is used mainly due to the similarity with the structure and properties of human bone, faster biological degradation, as well as the ability to transport damaged tissues of body fluids, which can significantly shorten the necessary regeneration time.[10,13]

A suitable approach in the design of biodegradable implants for medical purposes may be to combine the good mechanical properties of metallic biomaterials with the biocompatibility and degradation properties of polymeric biomaterials by applying polymeric coatings to metals. Due to its high solubility in aqueous media, good biocompatibility, biodegradability, hydrophilicity, and mechanical properties similar to those of some soft tissues, polyethylene glycol (PEG) is suitable for biomedical applications including surface modification, bioconjugation, drug delivery, and tissue engineering. Moreover, PEG can be attached to the surface of drug-encapsulating materials to increase stability and solubility in vivo and reduce the rate of degradation from the bloodstream, thereby optimizing the efficacy of the administered drug.[14−17]

Surface coating can also improve antibacterial properties to prevent any postoperative infections,[18,19] which are among the most common complications after surgery and may be dangerous to patients. Bone infections are among the main problems that occur when a foreign body is implanted in the physiological environment. The use of drug delivery systems specifically is an effective means of treating local infections.[20−22] Antibiotics such as vancomycin or gentamicin have been popularized for local antibiotic administration by incorporating these antibiotics into bone cement used to fix prosthetic implants. However, several recent studies have reported that these antibiotic-loaded bone cements are not very effective. Controlled antibiotic-release coatings based on biodegradable materials are, therefore, becoming a possible alternative. Biodegradable coatings with an antibiotic content on the surface of the implants support the release of the drug during the degradation of the surface layers that reach the interface of the implant surface and tissue.[23]

Gentamicin sulfate is an aminoglycoside antibiotic used mainly to deal with bone infections due to its relatively broad antimicrobial spectrum and high thermostability.[21,24,25] Research by Nichol et al. revealed that the addition of gentamicin to a monolayer organic–inorganic hybrid sol–gel coating completely eradicated planktonic bacteria as well as biofilms of a panel of clinically relevant staphylococci, while such a coating did not interfere with bone healing.[26] Likewise, high- and long-term doses of gentamicin can trigger serious adverse reactions in the surrounding nerves, so it is important to choose only the necessary concentration of the drug for the given time.[27] Since bacterial colonization usually occurs in the first hours after material implantation, short-term systemic prophylaxis is as effective as long-term prevention. In fact, a short-term local drug delivery system can meet the requirements to prevent local infection while limiting possible long-term adverse side effects.[28]

The application of polymeric and bioactive antibiotic coatings (containing gentamicin sulfate) on iron substrates represents a new concept for improving degradation and biocompatibility. The combination of an iron-based sample, a polymer PEG coating, and an antibiotic (gentamicin sulfate) also represents a promising concept in terms of antibacterial properties, which have not been sufficiently investigated for these materials. *Staphylococcus aureus* is one of the most common pathogenic bacteria that causes local infection.[29] Both porous foam iron samples and solid iron samples in the form of pellets with a bare polymeric and bioactive coating containing gentamicin were prepared in this work and then examined for degradation properties, as well as cytotoxicity and antibacterial properties. The obtained results demonstrated the suitability of the prepared materials for potential use in health care, mainly due to their suitable degradation properties, good biocompatibility, and antibacterial properties.

https://doi.org/10.1021/acsomega.4c01002
ACS Omega 2024, 9, 27113−27126

2. MATERIALS AND METHODS

2.1. Iron Foam Preparation. Foam iron samples (fFe) were prepared by pouring PUR (polyurethane) foam (Filtren, Czech Republic) cylinders with a diameter of about 1 cm into a suspension prepared by dissolving 0.2 g of gelatin (Sigma-Aldrich, USA) in 6 mL of distilled water and then adding of carbonyl iron powder, (BASF, type CC d50, fraction 3.8−5.5 μm) which was used as the base material. The suspension-impregnated cylindrical samples were sintered in an Aneta 1 tube furnace (ANETA, Trenčianská Teplá, Slovakia) in two steps. The first step, at 450 °C for 120 min in an inert atmosphere (N_2) to remove the PUR foam. The second step, the sintering of the suspension-impregnated cylinders themselves at 1120 °C, for 60 min took place in a reducing atmosphere of hydrogen (heating rate 5 °C/min, cooling rate 4−5 °C).

2.2. Iron Compact Preparation. Compact samples (cFe) were prepared from carbonyl iron powder (CIP, BASF, type CC d50, fraction 3.8−5.5 μm) by cold pressing into pellets with a diameter of 12 mm at a pressure of 600 MPa. The pressed samples were then sintered at 1120 °C in a reducing atmosphere of hydrogen for 1 h.

2.3. Surface Modification of the Prepared Material. *2.3.1. Deposition of Polymer Coating on the Iron Samples.* The surface of both the porous foam iron samples and the compact iron samples was modified with a poly(ethylene glycol) 4000 (Sigma-Aldrich, USA) coating layer. An ethanol solution containing 10 wt % PEG was prepared. The samples were first cleaned with sandpaper and then ultrasonically for 10 min in acetone and ethanol and then immersed in the PEG solution for 3 h at room temperature and dried for another 3 h at 45 °C (Figure 1a). The samples were marked as fFe-PEG and cFe-PEG.

2.3.2. Deposition of Bioactive Coating on Iron Samples. A part of the foam and compact iron samples was modified with a polymeric bioactive coating consisting of PEG and gentamicin (Figure 1b). An ethanol solution was prepared containing 10 wt % PEG and 300 mg of gentamicin sulfate (cell-culture tested, 590 μg of gentamicin base/mg, Sigma G-1264) for 50 mL of solution.

The compact samples were first cleaned with sandpaper and then ultrasonically for 10 min in acetone and ethanol and then immersed in the PEG solution containing gentamicin for 3 h at room temperature and dried for another three h at 45 °C. The samples were marked as fFe-PEG + Ge and cFe-PEG + Ge.

2.4. Characterization of Materials. *2.4.1. Surface Morphology and Composition.* Macroscopic images of the prepared materials were taken with a Dino-Lite Premier AM4013MT digital microscope (1.3 MPx, 20× magnification).

The morphology of the prepared samples was studied by scanning electron microscopy (SEM) and the surface composition by energy dispersion analysis (EDX) (JEOL JSM-7000F, Japan with EDX INCA).

The specific surface area of the samples was determined by the low-temperature nitrogen adsorption method, and the specific surface area values of the tested samples (values represent the average of five measurements) were obtained using the Brunauer−Emmett−Teller (BET) method (NOVA 1200 e Surface Area and Pore Size Analyzer, Quantachrome Instruments, London, UK).

FTIR (Fourier transform infrared spectroscopy) spectra were recorded on an infrared spectrometer by using the ATR (Attenuated Total Reflectance) method (Bruker Optik GmbH, Ettlingen, Germany).

The porosity of the prepared foam materials was determined by using ImageJ software. To calculate the porosity of the iron samples, the SEM images were converted to RGB format and digitized in an ImageJ Analyzer. Pixel segmentation was then performed using a threshold formula distinguishing between black pixels (porosity) and gray pixels (sample), allowing the total optical porosity to be quantified.[30]

XPS (X-ray photoelectron spectroscopy) data were recorded using a Thermo Scientific K-Alpha XPS system (Thermo Fisher Scientific, UK) equipped with a microfocused monochromatic Al Kα X-ray source (1486.6 eV). A 400 μm X-ray beam at 6 mA × 12 kV was used. Spectra were acquired in the constant energy mode of the analyzer with a pass energy of 200 eV for the survey. Narrow regions were collected with a pass energy of 50 eV, with an energy step size of 0.1 eV. The Thermo Scientific Advantage software, version 5.9931 (Thermo Fisher Scientific), was used for digital acquisition and data processing. The surface composition (atomic %) was determined by considering the integrated peak areas of the detected atoms and the corresponding sensitivity factors. Each spectrum represents the average of the three measurements.

2.4.2. Electrochemical Measurements. The prepared materials were subjected to a dynamic degradation test by means of an anodic polarization method using an Autolab PGSTAT 302N potentiostat. A three-electrode system was used in which the prepared sample was a working electrode, a silver chloride electrode (Ag/AgCl/KCl (3 mol/L) was a reference electrode, and a platinum electrode was used as an auxiliary electrode. The potentials were scanned in the range from -400 to -800 mV at a scan rate of 0.1 mV/s. During the test, the samples were immersed in Hanks' solution, which is used as a simulated physiological environment. It is a balanced salt solution that mimics the ionic composition of human extracellular fluid and provides a suitable environment for evaluating material degradation and biocompatibility (with composition: 8 g/L NaCl; 0.4 g/L KCl; 0.14 g/L $CaCl_2$; 0.1 g/L $MgSO_4{\cdot}7H_2O$; 0.1 g/L $MgCl_2{\cdot}6H_2O$; 0.06 g/L $Na_2HPO_4{\cdot}2H_2O$; 0.06 g/L KH_2PO_4; 1 g/L Glucose; 0.35 g/L $NaHCO_3$, and pH = 7.4 ± 0.2) and tempered at 37 ± 2 °C.

Three samples were studied for each analysis. The corrosion rate was subsequently calculated using the Tafel extrapolation method according to eq 1 based on ASTM G59:[31]

$$\mathrm{CR} = \frac{j_{\mathrm{corr}}\mathrm{KEW}}{d} \tag{1}$$

where CR is the corrosion rate (mm/year), j_{corr} is the current density (A/cm^2), K is the constant determining the resulting units, EW is the equivalent weight of the material, and d is the material density (g/cm^3).

After the measurement, the samples were removed from the Hanks' solution, rinsed with ethanol, and dried in air.

Prior to the start of the degradation tests, the open circuit potential (OCP) was recorded for 60 min after solution stabilization. The OCP value was used in the measurement of electrochemical impedance spectroscopy (EIS), which was performed with the same three-electrode system as for the electrochemical degradation test. The samples were immersed in 50 mL of Hanks' solution during the measurement. The measurement took place in the frequency range of 10 mHz−100 kHz with an alternating current amplitude of 10 mV. Gentamicin release tests were carried out using EIS and

https://doi.org/10.1021/acsomega.4c01002
ACS Omega 2024, 9, 27113−27126

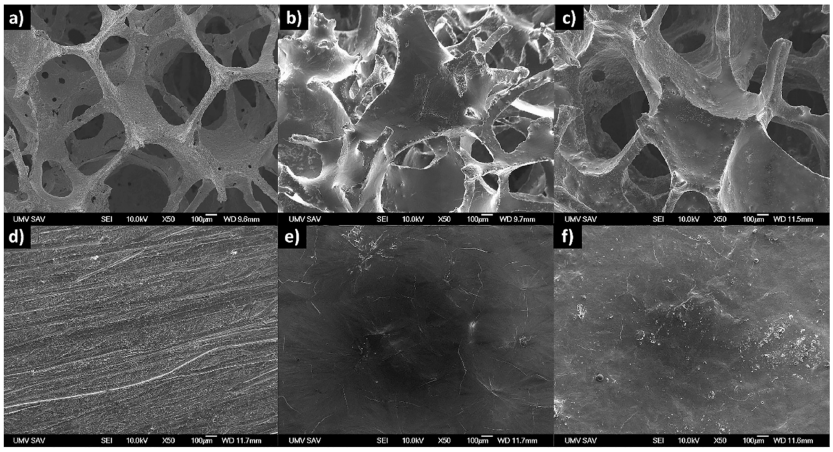

Figure 2. SEM images of foam and compact iron-based samples: (a) fFe, (b) fFe-PEG, (c) fFe-PEG + Ge, (d) cFe, (e) cFe-PEG, and (f) cFe-PEG + Ge.

conductivity measurements. EIS measurements were carried out by using Solartron Analytical Modulab (mdl. 2100 A), within the frequency range from 100 kHz to 1 Hz with amplitude 10 mV at the potential 15 mV vs reference electrode. The EIS measurement data were fitted and evaluated by using the Zview program. The PBS solution was used for EIS measurement, and distilled water was used for conductivity measurements. These measurements were performed via a WTW Inolab conductivity meter Level 1.

2.4.3. Immersion Degradation Tests. The immersion corrosion test was also performed in Hanks' solution. Prior to the start of the test, the samples were weighed (m_i) and then ultrasonically cleaned in acetone and ethanol for 10 min. Subsequently, the three sets of test samples were immersed in Hanks' solution. The first set of samples was subjected to an immersion corrosion test for 4 weeks, the second for 8 weeks, and the third for 12 weeks at 37 °C. Three samples from each species were studied in each set. At the end of the test, the samples were ultrasonically cleaned in acetone and ethanol for 10 min to remove the excess corrosion products, then air-dried and weighed (m_f). The corrosion rate was determined from the change in weight according to the eq 2 based on ASTM G31 standard:[32]

$$\mathrm{CR} = \frac{(m_i - m_f)K}{Atd} \tag{2}$$

where CR is the corrosion rate, m_f is the mass of the sample at the end of the test, m_i is the mass of the sample at the beginning of the test, K is constant (87600), A is the surface area of the sample, t is the exposure time, and d is the material density.

2.4.4. Cytotoxicity Test. The sample toxicity testing was performed in vitro according to STN ISO 10993-5 norm[33] at 37 °C. Samples of fFe, cFe, fFe-PEG, cFe-PEG, fFe-PEG + Ge, cFe-PEG + Ge, and stainless steel (SS) were sterilized by UV and placed in polypropylene (PP) centrifuge tubes, where 2 mL of the culture medium consisting of Dulbecco's modified Eagle's medium (DMEM) with 10% fetal bovine serum (FBS) and 1% antibiotic solution (ATB) was added. To obtain the extracts, the samples were immersed in the culture medium for two different time intervals, 4 and 24 h. Subsequently, samples were taken from the tubes and the obtained extracts were centrifuged for 5 min at 10,000 rpm.

The cell population was determined in a Bürker chamber prior to the experiments. Centrifuged extracts were subsequently used to determine the in vitro cytotoxicity. Human dermal fibroblast (Human Dermal Fibroblasts, HDFa; Sigma-Aldrich) cells were placed in a 96-well plate (Grade Brand culture microplate, adherent cells); 100 μL of culture medium was added to each well of the plate so that there was 10^4 HDFa in each cell. Cultivation until the formation of monolayers took place in an incubator (37 °C, 95% humidity, and 5% CO_2). After 24 h of incubation, the culture medium from each well was removed and subsequently, prepared extracts were added to the wells with seeded cells and were left for incubation for 4 h. After incubation, the extract from each well was pipetted off and the cytotoxicity was determined by MTS proliferation assay (CellTiter 96 AQueous one solution cell proliferation assay, Promega, USA). 100 μL of MTS reagent was placed in each well of the plate, which was placed in an incubator at 37 °C for 4 h. Afterward, the absorbance of formazan was determined at 490 nm using UV VIS spectrophotometer (Shimadzu), and then cell viability was calculated using eq 3:

$$V(\%) = \frac{\mathrm{OD}}{\mathrm{OD_{NC}}} \times 100\% \tag{3}$$

where OD is the optical density of the iron samples and $\mathrm{OD_{NC}}$ is the optical density of the negative control. The experiment was repeated three times for each sample using wells without extracts as a negative control.

2.4.5. Antibacterial Activity Test. The antibacterial activity of Fe-PEG and Fe-PEG + Ge was tested against bacterial strains of *Escherichia coli* CCM 3954 and *Staphylococcus aureus* CCM 4223 (Czech Collection of Microorganisms, Brno).

2.4.5.1. Disc Diffusion Method. The bacterial strains tested to determine the antibacterial activity of Fe-PEG and Fe-PEG + Ge were cultivated for 18 h. Subsequently, the suspensions were prepared in a sterile physiological solution and adjusted to a value of 0.5 on the McFarland scale. The thus-prepared suspensions were inoculated on Mueller–Hinton agar (MHA) in a volume of 100 μL. Consequently, 10 μL of PEG and PEG + Ge were added on paper discs with a diameter of 6 mm in a concentration range from 6 to 0.047 mg/mL. Antibacterial activity was evaluated by measuring the diameter of the inhibition zone in millimeters. An antibiotic disc with gentamicin (10 μg) was used as a control.

https://doi.org/10.1021/acsomega.4c01002
ACS Omega 2024, 9, 27113−27126

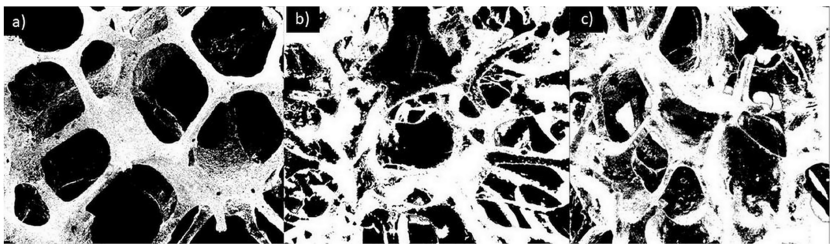

Figure 3. Porosity determination of foam (a) fFe, (b) fFe-PEG, and (c) fFe-PEG + Ge samples using ImageJ software.

2.4.5.2. Spectrophotometric Test. The antibacterial activity of the Fe-PEG + Ge solution was determined spectrophotometrically by measuring the absorbance. The PEG + Ge solution was diluted in BHI (Brain-Heart Infusion) broth in 96-well plates in a concentration range of 150−4.7 μg/mL. The tested bacterial strains were cultivated for 18 h, and the prepared suspensions in a sterile physiological solution were adjusted to a value of 1.0 on the McFarland scale. Subsequently, the bacterial suspensions were added to the diluted PEG + Ge solution in a ratio of 1:1. After 24 h of incubation at 37 °C, the antibacterial activity was spectrophotometrically determined by measuring the absorbance at a wavelength of 600 nm using a Biotek Synergy 2 device. BHI broth with the tested bacterial strains was used as a control. The results were evaluated by using the Dunnett test in the statistical program Prism 8.3.0.

3. RESULTS AND DISCUSSION

3.1. Morphology and Surface Composition. SEM images of the surface of the prepared foam and compact (Figure 2) materials were taken as further confirmation of the presence of the polymeric coating. Both the micropores (with a size from 0.5 to 5 μm) and macropores (with a size from 450 to 1500 μm) were present in the prepared foam samples.

In the case of coated iron foams, the macropore size decreased, and the walls thickened as compared to the uncoated foam samples. As a result of the coating deposition, the cells were partially or wholly filled with polymer, and the macropores were reduced or completely closed. Moreover, the deposition of the PEG coating caused the micropore closure, smoothing out the structure and creating a glossier and smoother surface of the material. These changes in the surface of the coated samples are well observable from the SEM images depicted in Figure 2b,c. The presence of scratches on the surface of the uncoated compact samples (Figure 2d) was observed due to the cleaning of the material with sandpapers prior to coating. Application of the pure PEG coating as well as the coating containing gentamicin resulted in the smoothing of the surface of the material (Figure 2e,f).

The porosity of the prepared foam samples was determined to be 56.23% (Figure 3a), 44.97% (Figure 3b), and 41.32% (Figure 3c) for the fFe, fFe-PEG, and fFe-PEG + Ge samples, respectively. Black areas in Figure 3 show the pores that are present.

To examine the surface properties of the prepared foam samples, we determined the specific surface area values (S_{BET}) of the samples were determined. The results are shown in Table 1. The specific surface area values for the fFe-PEG and fFe-PEG + Ge samples were lower by almost half compared to the uncoated Fe, which is related to the smoothing of the surface and the reduction of the pore size of the polymer-coated samples.

Table 1. Specific Surface Area Values of Porous Foam Samples

sample	S_{BET} (m^2/g)
fFe	0.34
fFe-PEG	0.17
fFe-PEG + Ge	0.21

The surface areas of the compact samples were determined by geometric calculation. The average surface area of the compact samples was 3.18×10^{-4} m^2 which corresponds to a specific surface area of approximately 1.59×10^{-4} m^2/g.

The presence of a polymeric PEG coating layer on the surface of the coated samples was confirmed by the surface EDX analysis based on the presence of oxygen and carbon on the surface of the analyzed cFe-PEG, fFe-PEG, cFe-PEG + Ge, and fFe-PEG + Ge samples, which were not observed in the case of pure iron. Nitrogen and sulfur were not detected on the surface of any foam samples due to their low content. In the case of the compact cFe-PEG + Ge sample, the pre-presence of sulfur was detected to confirm the gentamicin sulfate on the surface. The average values of the content of individual elements on the surface are listed in Table 2. In the case of the fFe-PEG + Ge sample, the presence of iron was observed on the surface, which was caused by the uneven distribution of the coating on the sample surface and the tips of Fe nodes protruding from the coating layer. In the case of uncoated iron samples (fFe and cFe), only Fe was observed on the surface.

The presence of the polymer coating was also confirmed by infrared spectroscopy. Figure 4a shows the infrared spectra of the pure PEG, Ge, Fe, Fe-PEG, and Fe-PEG + Ge samples. In the infrared spectrum of pure PEG, functional group vibrations were identified as follows: valence vibrations of the −OH group at 3400 cm^{-1}, asymmetric and symmetric valence vibrations of the $-CH_2$ group at 2869 cm^{-1}, valence vibrations of the −CO group at 1099 cm^{-1} and deformation vibrations of CH groups at 960 and 840 cm^{-1}. The absorption bands at 1461, 1359, and 1280 cm^{-1} further characterize the deformation vibrations of CH_2 groups. The presence of a triple peak of valence vibrations C−C and C−O in the range from 1000 to 1200 cm^{-1} is evidence of the existence of a crystalline phase and was found in the spectrum of pure PEG as well as in Fe-PEG and Fe-PEG − Ge samples.[34]

In the infrared spectrum of pure gentamicin, functional group vibrations were identified as follows: the amide (N−H) bending vibrations of primary aromatic amines at 1620 and 1524 cm^{-1} and the S−O bending vibration and S−O stretch at 600 and 1040 cm^{-1}.[35] No gentamicin peaks were detected in the spectrum of the Fe-PEG − Ge sample due to the low content of gentamicin in the polymer coating; therefore, PEG peaks predominated in the sample.

https://doi.org/10.1021/acsomega.4c01002
ACS Omega 2024, 9, 27113−27126

Table 2. Surface Composition of Fe, Fe-PEG, and Fe-PEG − Ge Samples Determined by EDX Analysis

	Fe		C		O		S	
	wt %	at %	wt %	at %	wt %	at %	wt %	at %
				foam samples				
fFe	100	100						
fFe-PEG			62.27	68.73	37.73	31.27		
fFe-PEG + Ge	16.56	4.44	56.04	69.90	27.40	25.66		
				compact samples				
cFe	100	100						
cFe-PEG			64.08	70.38	35.92	29.62		
cFe-PEG + Ge			64.17	70.46	35.83	29.54	0.41	0.33

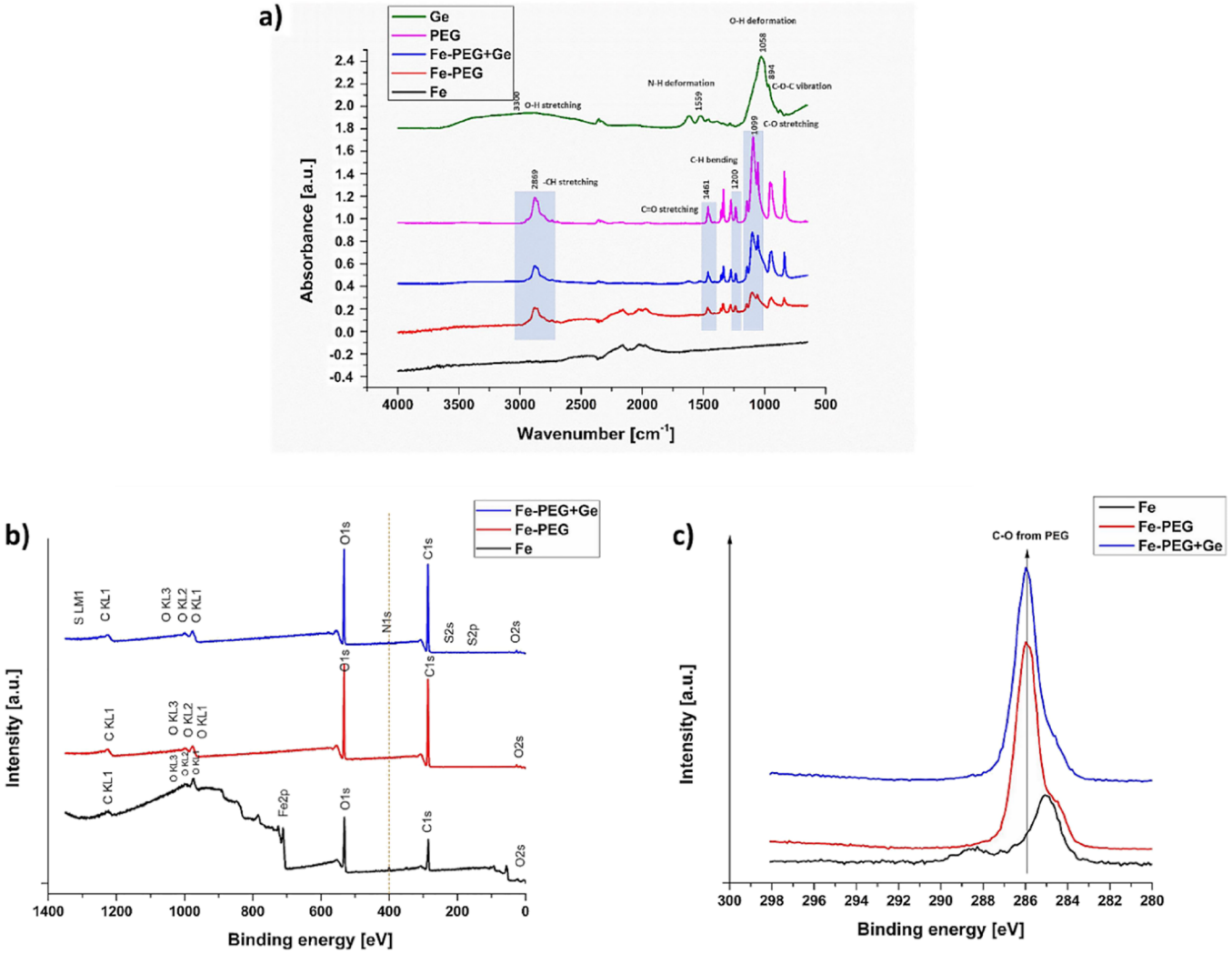

Figure 4. (a) Infrared spectrum of the prepared studied materials − Fe, Fe-PEG, Fe-PEG + Ge, pure polyethylene glycol (PEG), and gentamicin sulfate (Ge), (b) survey XPS spectra of prepared Fe, Fe-PEG, and Fe-PEG + Ge samples, and (c) survey XPS spectra of prepared Fe, Fe-PEG, and Fe-PEG + Ge samples.

Moreover, XPS analysis was performed to further examine the chemical state of elements present at the sample surface. In the case of the Fe sample, the presence of peaks corresponding to oxygen on the surface due to the formation of iron oxides (the main Fe 2p signal at 710.9 eV corresponding to iron oxides, Figure 4b, Table 3) on the surface of the sample was observed.

In the Fe-PEG sample, the surface was almost completely covered with polymer; therefore, only peaks corresponding to

Table 3. Apparent Surface Chemical Composition Determined by XPS

sample	surface chemical composition (at %)				
	C 1s	O 1s	Fe 2p	N 1s	S 2p
Fe	46.4	41.2	10.2	2.3	
Fe-PEG	78.5	21.5			
Fe-PEG + Ge	68.1	30.9		0.7	0.3

https://doi.org/10.1021/acsomega.4c01002
ACS Omega 2024, 9, 27113−27126

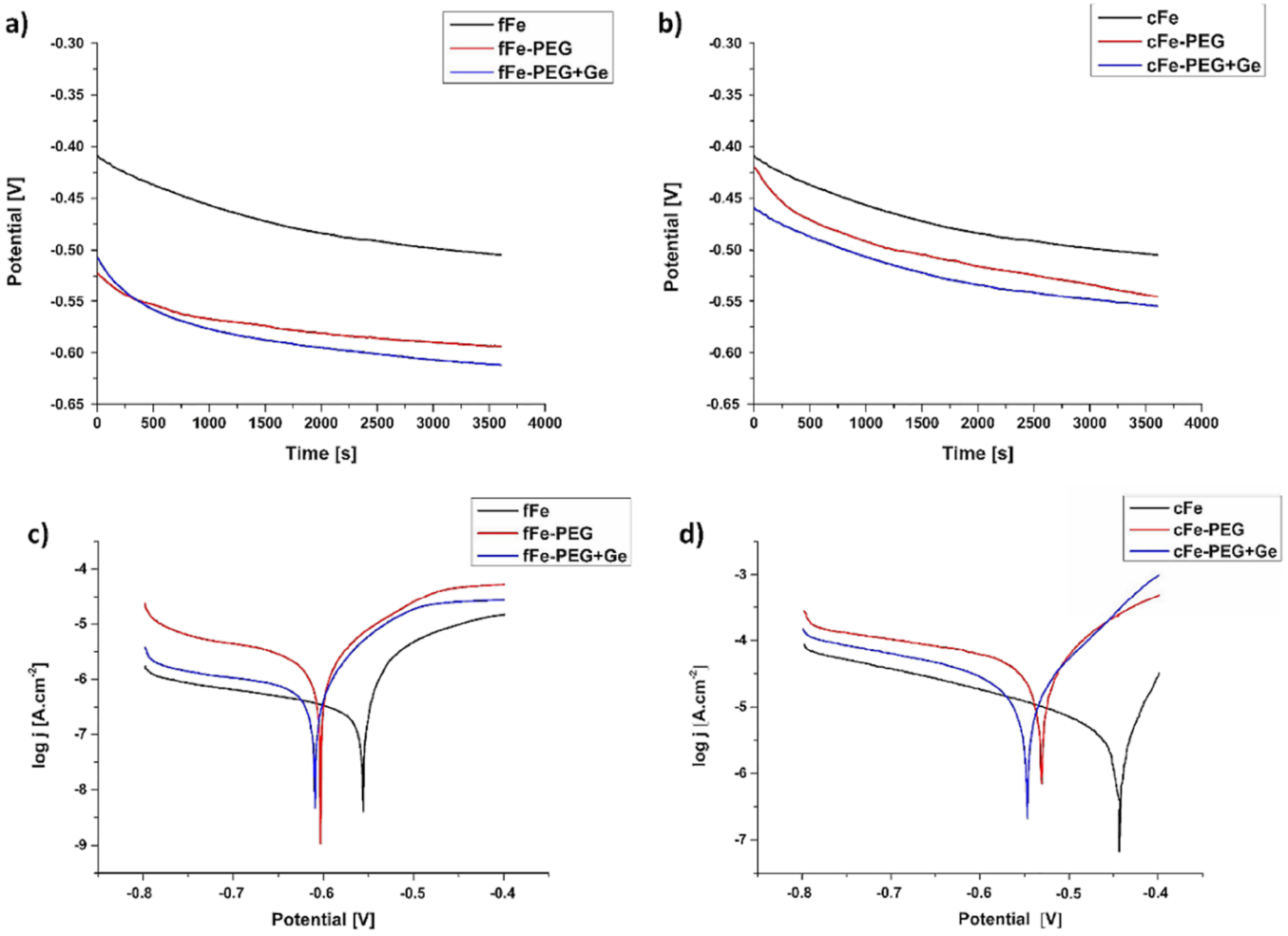

Figure 5. Time dependence of the OCP for (a) foam iron-based samples, (b) compact iron-based samples, and potentiodynamic polarization curves of (c) foam, and (d) compact samples Fe, Fe-PEG, and Fe-PEG + Ge in Hanks' solution.

oxygen and carbon from the PEG coating were observed (see Figure 4c, C 1s at ca. 286.0 eV confirms C−O from PEG). Based on the S 2p and N 1s peaks, the presence of gentamicin in the Fe-PEG + Ge sample was confirmed.

Some nitrogen was also observed in the case of the Fe sample, which is mainly at ca. 400.0 eV, corresponding to the C−N group. This probably comes from some contamination of the Fe surface. In the case of the Fe-PEG + Ge sample, N 1s is mainly at 401.1 eV, corresponding to $-NH_3^+$ and S 2p is at ca. 168.2 eV, corresponding to sulfate. This clearly confirms the presence of charged gentamicin sulfate on the surface.

Fe-PEG + Ge is fully coated by PEG (68.1 at % of carbon with main C−O signal at 286.0 eV, Table 3, Figure 4c). A certain amount of gentamicin is bound to the surface of this layer. Similar results were observed in studies where the presence of surface-bound drugs (gentamicin) was observed on microspheres produced using polylactic acid (PLLA) and copolymer of lactic acid and glycolic acid (PLGA).[36,37]

3.2. Corrosion Behavior. *3.2.1. Electrochemical Corrosion Behavior.* The OCP potential was registered for 60 min. After about 40 min, the OCP values stabilized in the range from −0.54 to −0.62 V for each porous foam sample (Figure 5a) and in the range from −0.48 to −0.57 V for each compact sample (Figure 5b). The lowest OCP values were observed for the fFe-PEG, cFe-PEG, fFe-PEG + Ge, and cFe-PEG + Ge samples. This indicates an increased tendency to corrosion in the coated samples.

To determine the corrosion rate (CR), dynamic polarization tests were performed in Hanks' solution at 37 °C. Table 4 shows the values of corrosion potential (E_{corr}), corrosion current density (j_{corr}), and CR values determined by the Tafel extrapolation method from the potentiodynamic polarization curves (Figure 5c, d). A potential shift to a more negative value was observed for both compact and foam samples with the PEG coating and the PEG coating containing gentamicin, indicating a higher tendency to corrosion compared with the uncoated samples.

Table 4. Values of j_{corr}, E_{corr} and Corrosion Rates for the Fe, Fe-PEG, and Fe-PEG − Ge Samples

	E_{corr} (mV)	j_{corr} (μA·m^{-2})	CR(mmpy)
foam samples			
fFe	−558	28.685	0.333
fFe-PEG	−604	62.555	0.727
fFe-PEG + Ge	−610	64.750	0.752
compact samples			
cFe	−444	25.319	0.294
cFe-PEG	−532	47.543	0.552
cFe-PEG + Ge	−548	55.264	0.642

https://doi.org/10.1021/acsomega.4c01002
ACS Omega 2024, 9, 27113−27126

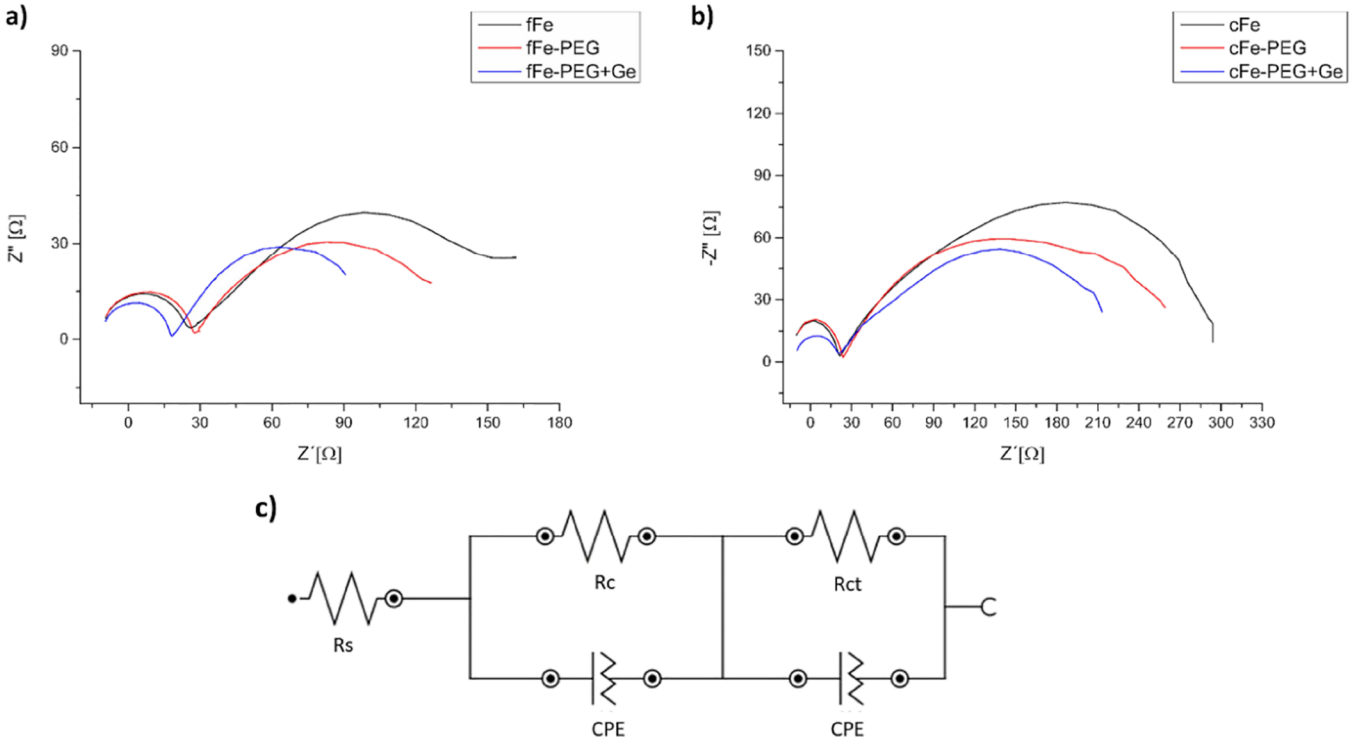

Figure 6. Nyquist diagram of (a) foam, (b) compact iron-based Fe, Fe-PEG and Fe-PEG + Ge samples before corrosion and (c) equivalent circuit – R_s – solution resistance, R_c – polymer layer resistance, R_{ct} – charge transfer resistance, CPE – elements of a constant phase.

The increase in the corrosion rate of the coated samples as compared to the uncoated sample can be attributed to the slight acidity of the corrosion medium in the vicinity of the surface of the coated samples due to the oxidative degradation of PEG.

The degradation of PEG begins with oxidation of the terminal OH group and splitting of the hydrogen atom, which leads to a decrease in the pH of the solution. The change in pH is also caused by the interaction between the polymer and water. A local reduction of the pH value near the surface of the coated samples subsequently leads to increased solubility of corrosion products and the formation of a less compact and dense passive layer, which accelerates their degradation.[38] The acidic environment leads to increased proton reduction at the cathode, which can cause higher corrosion current density and thus a higher corrosion rate.[39,40] When iron-based substrates with polyethylene glycol (PEG) coating are exposed to Hanks' solution, the corrosion rate increases due to the enhanced oxidation rate of iron caused by the interaction between the hydrophilic polymer layer and the iron surface.[41,42] However, it is also possible to influence the time of its degradation by the thickness of the polymer layer and thus adjust the properties of the biomaterial according to the requirements of the given application.

Nyquist diagrams of the prepared samples obtained before and after 60 min immersion in Hanks' solution are shown in Figure 6a,b. The diagrams demonstrate that the iron-based samples exhibit two types of loops: a capacitive loop in the high and medium frequency range and the induction loop in the low-frequency range. The capacitive loop is related to charge transfer, and the inductive loop is caused by the dissolution of iron.[43] For the foam as well as the compact samples, the high-frequency capacitive loop was described using the capacitance and charge transfer resistance, which characterized the bulk layer of the corrosion products.[44]

The occurrence of the semicircle in the low-frequency range reflects the surface inhomogeneity of the samples prepared by the powder metallurgy method. The semicircle diameters for the cFe and fFe samples are larger than those for the cFe-PEG, fFe-PEG, cFe-PEG + Ge, and fFe-PEG + Ge samples, indicating higher charge transfer resistance. The Nyquist diagrams of the uncoated and coated samples were modeled using the equivalent circuit shown in Figure 6c. In this circuit, R_s represents the solution resistance, R_c represents the polymer layer resistance, R_{ct} represents the charge transfer resistance, and CPE are elements of a constant phase.

The R_{ct} values, which represent the polarization resistance, were calculated for all samples as the difference in impedance at lower and higher frequencies (Table 5). The values for foam and the compact samples with the PEG coating layer as well as for foam and the solid samples containing gentamicin were lower than those for samples without the polymer layer indicating lower resistance to corrosion, which confirms the same trend as potentiodynamic polarization measurements

Table 5. Impedance Parameter R_{ct} for Foam and Compact Fe, Fe-PEG, and Fe-PEG + Ge Samples

	R_{ct} [Ω·m^{-2}]	
	foam samples	compact samples
Fe	168.93	312.74
Fe-PEG	114.90	254.41
Fe-PEG + Ge	100.07	235.21

Higher R_{ct} values for uncoated cFe and fFe samples indicate the formation of a passivation layer of degradation products, such as iron oxides, iron hydroxides, and carbonates, while

https://doi.org/10.1021/acsomega.4c01002
ACS Omega 2024, 9, 27113−27126

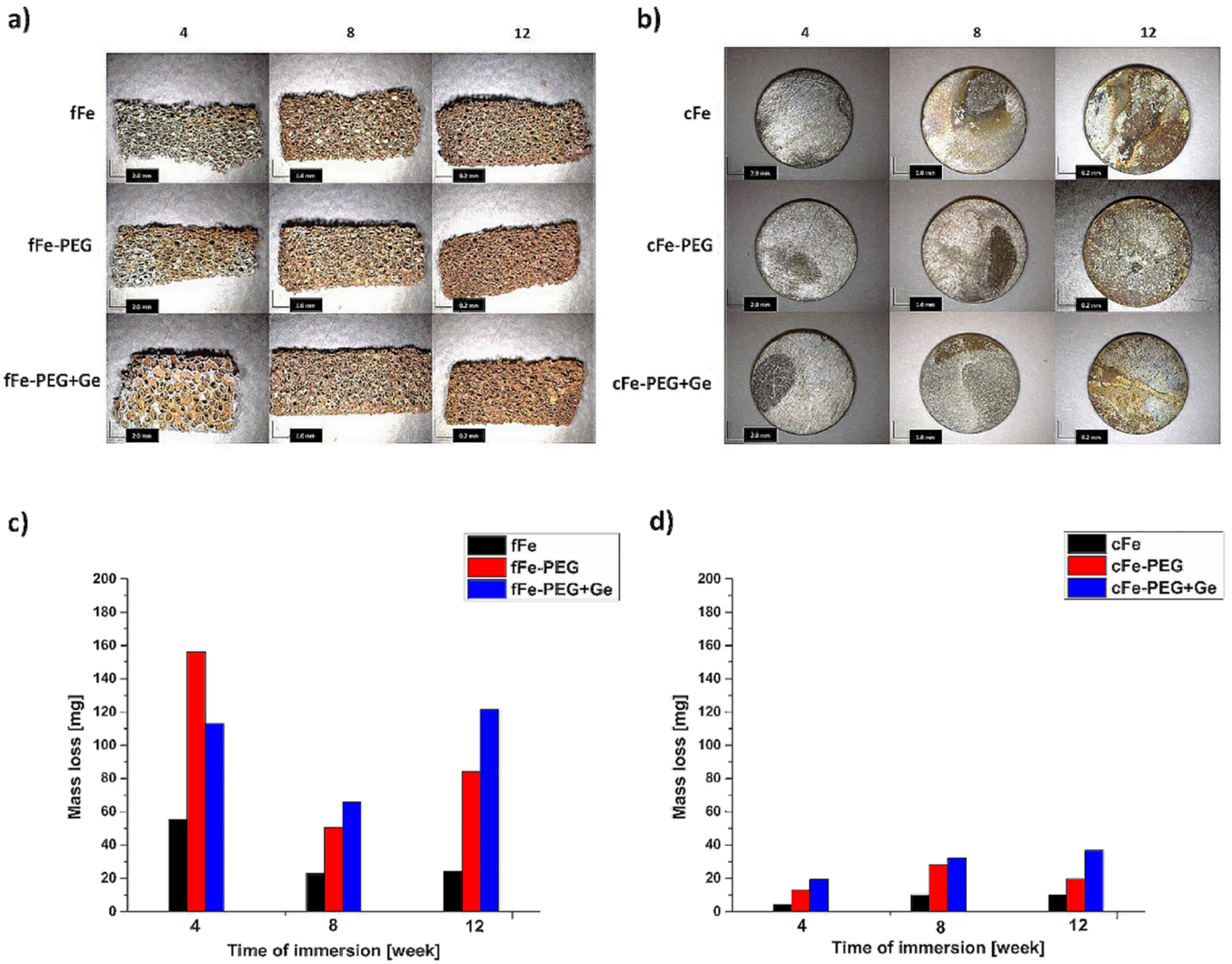

Figure 7. Macroscopic images of iron-based samples after 4, 8 and 12 week immersion in Hanks' solution at magnifications of 20×, (a) foam, (b) compact samples and mass losses during immersion in Hanks' solution for 4, 8, and 12 weeks for iron-based (c) foam (fFe, fFe-PEG, fFe-PEG + Fe) (d) compact (cFe, cFe-PEG, cFe-PEG + Ge) samples.

lower values obtained for the coated compact (cFe-PEG, cFe-PEG + Ge) and foam (fFe-PEG, fFe-PEG + Ge) samples indicate the desired higher corrosion rate.

The discrepancy between the increase in the R_{ct} value for the foam fFe-PEG + Ge and compact cFe-PEG + Ge samples compared with the fFe and cFe samples may be related to the complex nature of the layer formed and the partial breakdown of the surface film in some areas due to the addition of the antibiotic.

3.2.2. Immersion Corrosion Behavior. The static immersion degradation method was also used to determine the rate of degradation. The macroscopic images of the surface of the materials after immersion in Hanks' solution for 4, 8, and 12 weeks are shown in Figure 7a,b.

After 4 weeks of continuous immersion corrosion testing, it was still possible to observe several uncorroded sites on the surfaces of corroding samples. A thin layer of orange and brown corrosion products was visible on the surface of the Fe sample (Figure 7a). In the case of the fFe-PEG and fFe-PEG + Ge samples, a more pronounced coverage of the samples with corrosion products was observed. After 12 weeks of corrosion, the foam samples were relatively fragile; the walls of the samples were significantly damaged, and the surfaces of the samples were almost completely covered with a layer of corrosion products. The same trend was observed for compact samples (Figure 7b). However, even after 12 weeks of corrosion, the compact samples kept their shape relatively intact, which is due to the significantly smaller porosity and several times smaller surface area on which the corrosion took place.

The degradation rate for orthopedic implants depends on the specific application and requirements of implant. For small injuries, implants with accelerated degradation may lead to premature loss of mechanical support.[45] Conversely, in cases requiring medium-speed degradation, the use of implants with controlled degradation rates can ensure proper healing without compromising structural integrity.[46]

The biodegradation rate of the samples was determined by measuring the weight loss after immersion in Hanks' solution (Figure 7c,d). The calculated corrosion rates based on the continuous immersion test of both pressed and foamed samples after 4, 8, and 12 weeks are shown in Table 6. After 12 weeks of the immersion test, the degradation rate of pure fFe foam was 0.025 mm/year; the degradation rate of Fe

https://doi.org/10.1021/acsomega.4c01002
ACS Omega 2024, 9, 27113−27126

Table 6. Corrosion Rate of Prepared Samples Based on a Continuous Immersion Test

	CR (mmpy)					
	foam samples			compact samples		
	immersion time/week			immersion time/week		
sample	4	8	12	4	8	12
Fe	0.176	0.035	0.025	0.024	0.044	0.028
Fe-PEG	0.975	0.162	0.179	0.112	0.120	0.055
Fe-PEG + Ge	0.584	0.169	0.209	0.116	0.136	0.104

coated with the polymer coating (fFe-PEG) was 0.179 mm/year, and the degradation rate of Fe coated with the gentamicin-doped polymer coating (fFe-PEG + Ge) was 0.209 mm/year, which confirmed the required acceleration of the corrosion of the given material due to the polymer and bioactive coating. The highest weight loss was observed after 4 weeks of immersion in Hanks' solution for the fFe-PEG and after 12 weeks of immersion for the fFe-PEG + Ge foam samples.

Changes in CR with immersion time for samples with the polymer PEG layer as well as for samples with the PEG layer containing gentamicin were more significant compared to those of foams without a coating.

3.2.3. Gentamicin Release Tests. The gentamicin release was studied via both electrochemical impedance spectroscopy and measurement of the conductivity of the solution into which the drug was released. EIS measurements were performed every 15 s for 360 s for detailed study during the first minutes and then every 30 min for 72 h. Conductivity values were recorded continuously for 1 h.

The measurements were performed based on the assumption that the release of gentamicin into the electrolyte solution will affect its conductivity. At the same time, the degradation of the polymer film and the release of the drug will affect the interfacial electric properties that are possible to observe through EIS measurements. The decrease in the semicircle diameter can be seen in Figure 8 for all samples, indicating a decrease in charge transfer resistance. However, even in the case of a bare Fe sample without a coating and without a drug, a decrease in the charge transfer resistance (an increase in conductivity) was observed, which was caused by the dissolution of iron in the solution and the formation of Fe ions. After 1 h, it was possible to observe a slight increase in the charge transfer resistance. A similar trend can be observed in the case of the Fe-PEG sample, but the change in charge transfer resistance after 360 s was more pronounced (25 Ω) compared to that of the bare Fe sample (~15 Ω).

For the Fe-PEG + Ge sample, the change in charge transfer resistance after 360 s was even larger (approximately 30 Ω), which was related to the release of the drug from this coating. EIS measurements for sample Fe-PEG + Ge were performed also for a longer time scale of 72 h. The results of the measurements are shown in Figure 9b. During a wider time scale, the charge transfer resistance increases with the increasing time, but after 3 h, the values of charge transfer resistance are approximately constant.

For comparison, the release of the drug from the biomaterial sample was also studied by measuring the conductivity of the solution formed by dissolving the samples in distilled water. As can be seen in Figure 9a, the conductivity of distilled water has only a very slight increasing tendency with time for the Fe (from 1.3 to 2 μS/cm) and Fe-PEG samples (from 1.3 to 2.5 μS/cm). In the case of the Fe-PEG + Ge sample, a significant increase in conductivity at the very beginning of the measurement was observed: during the first 10 s, there was an increase from 1.3 to 8.2 μS/cm. This confirms the assumption that gentamicin is released from the surface of the sample immediately after immersion to a significant extent. However, the conductivity increases in the case of the Fe-PEG + Ge sample is nonuniform. These results suggest that drug release occurs in two steps. In the first step, the drug is released from the surface of the sample immediately after its immersion in the solution, and in the second step, the drug, which is embedded in the polymer coating, is gradually released. This conclusion is also supported by the results of EIS measurements, where the charge transfer resistance decreased during the first 360 s. This could be caused by the accumulation of a larger amount of gentamicin in the electrode space. But after a time, when it started to be released from places inside the polymer, the charge transfer resistance increased, because the conductivity of the polymer film on the electrode surface decreased since PEG is very poorly conductive.

3.3. Cytotoxicity. The MTS test was employed to evaluate the cytotoxicity of the porous foam and compact samples intended for potential application in the medical field. Figure 10 shows the viability of HDFa cells cultured in an extraction medium for 4 and 24 h. All extracts showed a decrease in cell viability compared with the negative control. After 4 h of incubation, cells cultured in the extracts of the PEG-coated foam sample showed the highest viability among the tested samples, while cells cultured in the extracts of the uncoated Fe

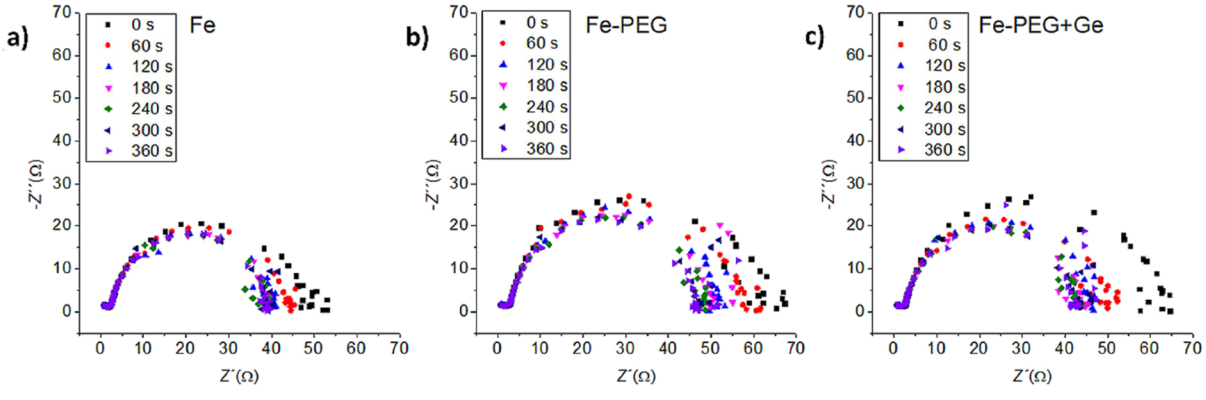

Figure 8. Nyquist diagrams for Fe (a), Fe-PEG (b), and Fe-PEG + Ge (c) samples during 360 s.

https://doi.org/10.1021/acsomega.4c01002
ACS Omega 2024, 9, 27113−27126

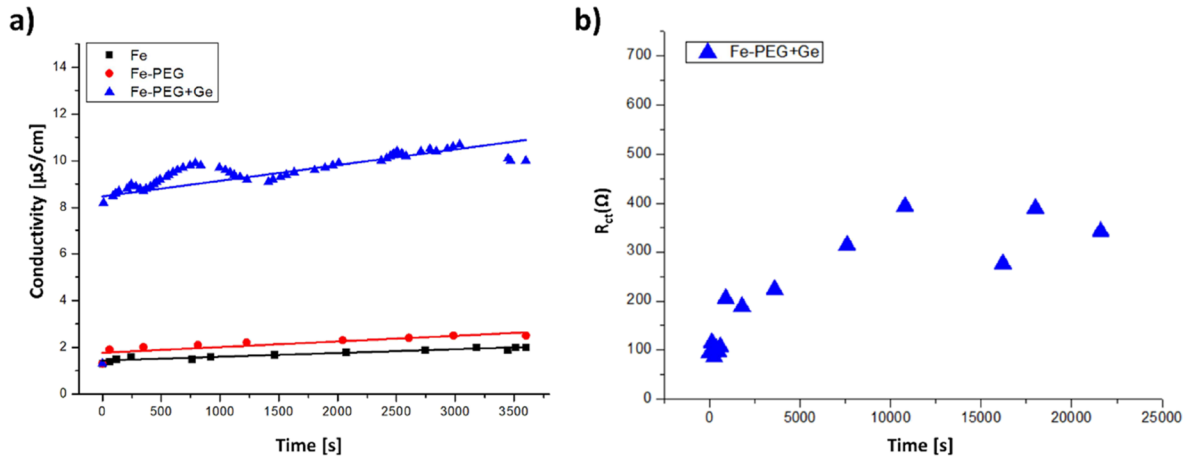

Figure 9. Solution conductivity changes during 1 h for Fe (black line), Fe-PEG (red line), and Fe-PEG + Ge (blue line) (a). Dependence of charge transfer resistance from time (b).

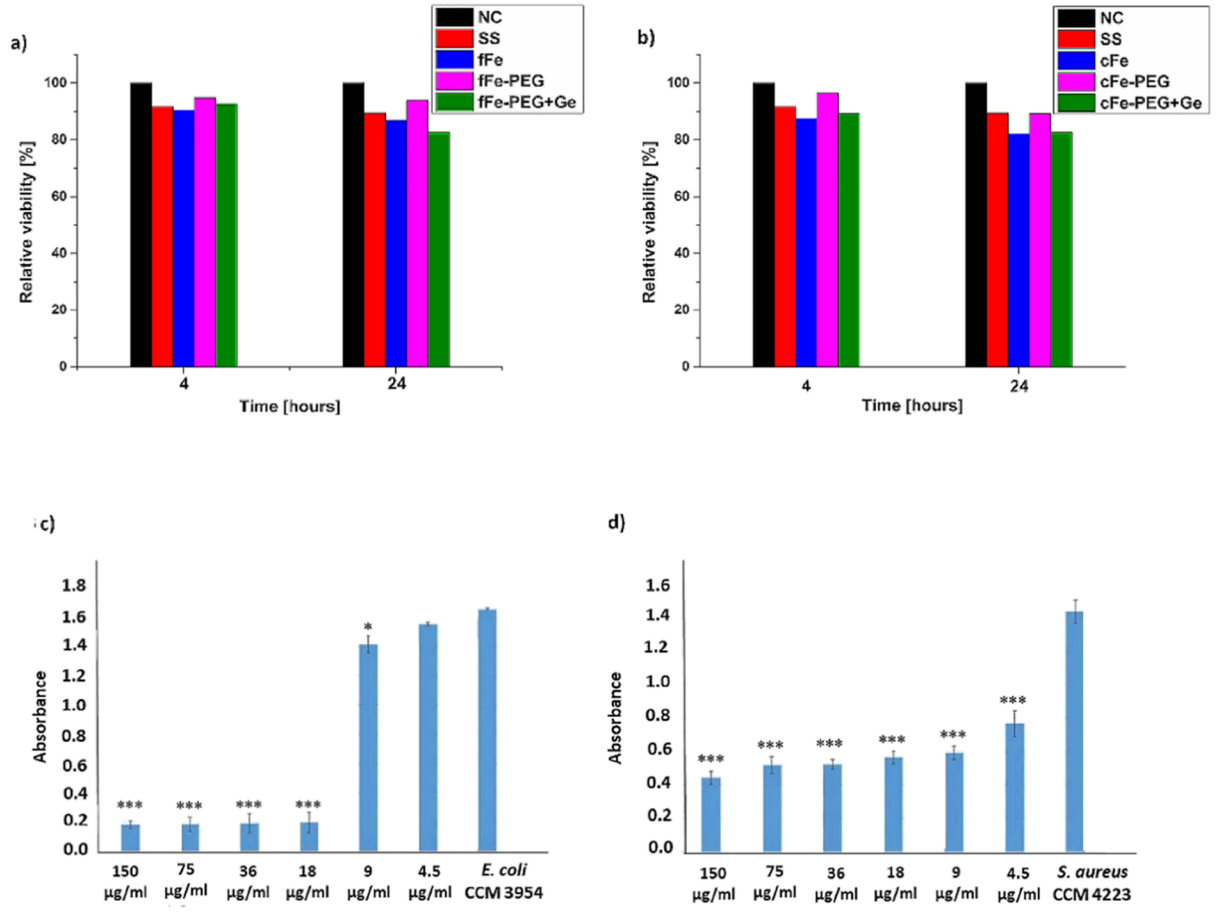

Figure 10. Relative viability of HDFa cells obtained from MTS assay after cultivation for 4 and 24 h in extraction mediums of (a) foam (fFe, fFe-PEG, fFe-PEG + Ge) and (b) compact (cFe, cFe-PEG, cFe-PEG + Ge) samples, stainless steel sheet (SS) and a negative control (NC) and antibacterial activity of Fe-PEG + Ge against (c) *Escherichia coli* CCM 3954 and (d) *Staphylococcus aureus* CCM 4223.

foam showed the lowest viability. The PEG-coated foam sample showed very low cytotoxicity with approximately 95% cell viability.

In the case of the fFe-PEG + Ge sample, the viability of HDFa cells was 93%. The relative cell viability in extracts from the fFe-PEG and fFe-PEG + Ge foams was about 3−5% higher than in the extract of the uncoated fFe sample. This indicates that the coating layer positively affected HDFa cell viability and promoted cell proliferation (Figure 10a). The same trend was observed for the compact samples (Figure 10b). For the compact cFe-PEG + Ge sample, a decrease in viability of 3% was observed compared with the foam fFe-PEG + Ge sample. With the prolonged incubation time, the cell viability started to decline, and after 24 h of cultivation, a decrease in viability below 90% was observed in all tested samples. A slight decrease of cell viability in extracts of the cFe-PEG + Ge and

https://doi.org/10.1021/acsomega.4c01002
ACS Omega 2024, 9, 27113−27126

fFe-PEG + Ge samples was observed compared to the PEG coating, although studies showed that gentamicin alone shows almost no decrease in viability compared to the control sample.[47]

3.4. Antibacterial Activity. The antibacterial activity of Fe-PEG and Fe-PEG + Ge was tested against *E. coli* CCM 3954 and *S. aureus* CCM 4223 using the qualitative diffusion method and the spectrophotometric dilution method. With the qualitative disc-diffusion method, the inhibitory activity was evaluated by measuring the inhibition zones in millimeters. An antibiotic disc with gentamicin (10 μg) was used as a control.

Based on the obtained results, no antibacterial activity was detected for Fe-PEG, but Fe-PEG + Ge showed antibacterial activity against *E. coli* CCM 3954 and *S. aureus* CCM 4223 in a concentration range from 6 to 0.18 mg/mL. Antibacterial activity was not detected at lower concentrations. The addition of gentamicin to the Fe-PEG sample coating provides some advantages such as better coating morphology, better biocompatibility with implants, and better antimicrobial effect. Biofilm-encrusted bacterial pathogens such as *S. aureus* and *E. coli* are major sources of bacterial infections and are very difficult to eradicate.

The antibacterial activity of PEG + Ge against *E. coli* CCM 3954 and *S. aureus* CCM 4223 was also tested using the spectrophotometric dilution method in microtiter plates by measuring the absorbance using Biotek Synergy 2. Concentrations from 150 to 18 μg/mL significantly suppressed the growth of *E. coli* CCM 3954 compared to the control (Figure 10c). Concentrations from 150 to 4.5 μg/mL significantly inhibited the growth of *S. aureus* CCM 4223 (Figure 10d). Regarding the antibacterial mechanism of action, a general mechanism with two following steps applies: an immediate and physically reversible step and a time-dependent irreversible molecular and cellular second step. In contact with a carrier such as tissue, competition occurs between microbial colonization and tissue integration.[48] The results confirmed that gentamicin, as an aminoglycoside antibiotic with broad-spectrum antibacterial effect can bind to anionic compounds on the surface of bacteria, causing their good antibacterial properties.[49]

4. CONCLUSIONS

Two different types of samples were prepared: porous foam samples and compact pellet samples. Samples with the bare PEG coating layer as well as with the bioactive coating were made to improve the degradation properties and the biocompatibility of the iron biomaterials. Samples coated with the polymeric layer (both bare PEG and PEG containing gentamicin) corroded faster compared to the uncoated samples. The reason for this acceleration was a local increase in the pH of the solution around the dissolved polymer, which led to an increased dissolution rate of the tightly adsorbed corrosion products and exposure to a new metal surface accessible for degradation. The faster degradation of the foam-coated samples was observed compared to the compact-coated samples, which was due to the larger surface area of the foam samples.

A significant increase in conductivity was observed in the case of the Fe-PEG + Ge sample compared with the Fe and Fe-PEG samples, which confirmed the release of gentamicin from the implant surface.

Cytotoxicity assays showed that cell viability decreased with increasing culture time for both coated and uncoated samples. A higher viability was observed for the cells cultured in the extracts of the foam samples compared to that in the compact samples. Tests to detect the antibacterial activity of Fe-PEG and Fe-PEG + Ge against *Escherichia coli* CCM 3954 and *Staphylococcus aureus* CCM 4223 proved that discs impregnated with Fe-PEG + Ge showed antibacterial activity against *E. coli* CCM 3954 and *S. aureus* CCM 4223 and spectrophotometrically showed significant antibacterial activity against both bacterial strains.

Research on gentamicin release and in vivo investigations of the biocompatibility of such materials will be the topic of our next study. In conclusion, increasing the rate of degradation of biomaterials in a simulated physiological environment and the promising resistance to basic strains of bacteria in the case of drug-doped coatings offers the possibility of using polymeric as well as gentamicin-doped coatings to improve the degradation properties of degradable iron-based biomaterials for application in the field of medicine.

■ ASSOCIATED CONTENT

Data Availability Statement

The data underlying this study are available in the published article. If additional data or information is needed, these are available from the corresponding author upon request.

■ AUTHOR INFORMATION

Corresponding Author

Renáta Oriňaková − *Department of Physical Chemistry, P. J. Šafárik University in Košice, 041 01 Košice, Slovakia; Centre of Polymer Systems, University Institute, Tomáš Bat'a University in Zlín, 76001 Zlín, Czech Republic;* orcid.org/0000-0001-8103-2634; Phone: +421-55-2342321; Email: renata.orinakova@upjs.sk; Fax: +421-55-6222124

Authors

Martina Petráková − *Department of Physical Chemistry, P. J. Šafárik University in Košice, 041 01 Košice, Slovakia*

Radka Gorejová − *Department of Physical Chemistry, P. J. Šafárik University in Košice, 041 01 Košice, Slovakia*

Jana Shepa − *Department of Physical Chemistry, P. J. Šafárik University in Košice, 041 01 Košice, Slovakia*

Ján Macko − *Department of Physical Chemistry, P. J. Šafárik University in Košice, 041 01 Košice, Slovakia*

Miriam Kupková − *Institute of Materials Research, Slovak Academy of Sciences, 040 01 Košice, Slovakia*

Matej Mičušík − *Institute of Polymers, Slovak Academy of Sciences, 845 41 Bratislava, Slovakia*

Matej Baláž − *Institute of Geotechnics, Slovak Academy of Sciences, 040 01 Košice, Slovakia;* orcid.org/0000-0001-6563-7588

Vanda Hajdučková − *Department of Microbiology and Immunology, University of Veterinary Medicine and Pharmacy in Košice, 041 81 Košice, Slovakia*

Patrícia Hudecová − *Department of Microbiology and Immunology, University of Veterinary Medicine and Pharmacy in Košice, 041 81 Košice, Slovakia*

Martin Kožár − *Small Animal Clinic, The University of Veterinary Medicine and Pharmacy in Košice, 040 01 Košice, Slovakia*

Barbora Šišková − *Small Animal Clinic, The University of Veterinary Medicine and Pharmacy in Košice, 040 01 Košice, Slovakia*

https://doi.org/10.1021/acsomega.4c01002
ACS Omega 2024, 9, 27113−27126

Petr Sáha − *Centre of Polymer Systems, University Institute, Tomáš Bat'a University in Zlín, 76001 Zlín, Czech Republic*

Complete contact information is available at: https://pubs.acs.org/10.1021/acsomega.4c01002

Author Contributions

M.P.: Writing, Investigation, Formal analysis, Visualization; R.G.: Validation J.S.: Investigation, Formal analysis; J.M.: Investigation, Methodology; M.K.: Investigation, Methodology; M.M.: Investigation, Formal analysis; M.B.: Investigation, Formal analysis; V.H.: Investigation, Formal analysis; P.H.: Investigation; M.K.: Investigation, Resources; B.Š.: Investigation; P.S.: Funding acquisition; R.O.: Supervision. All authors read and approved the final manuscript.

Notes

The authors declare no competing financial interest.

■ ACKNOWLEDGMENTS

This work was supported by Project APVV-20-0278 of the Slovak Research and Development Agency and from the agency VEGA 02/00006/22 (Slovakia). This work is supported by the Ministry of Education, Youth and Sports of the Czech Republic (DKRVO RP/CPS/2022/005), by the Internal scientific grant system of the Faculty of Natural Sciences UPJŠ in Košice (vvgs-2023-2518), and by the Visegrad Grants from International Visegrad Fund (project no. 22310096).

■ REFERENCES

(1) Li, Y.; Jahr, H.; Lietaert, K.; Pavanram, P.; Yilmaz, A.; Fockaert, L. I.; Leeflang, M. A.; Pouran, B.; Gonzalez-Garcia, Y.; Weinans, H.; Mol, J. M. C.; Zhou, J.; Zadpoor, A. A. Additively manufactured biodegradable porous iron. *Acta Biomater* **2018**, *77*, 380−393.

(2) Zhao, D.; Witte, F.; Lu, F.; Wang, J.; Li, J.; Qin, L. Current status on clinical applications of magnesium-based orthopaedic implants: A review from clinical translational perspective. *Biomaterials* **2017**, *112*, 287−302.

(3) Priyadarshini, B.; Rama, M.; Chetan; Vijayalakshmi, U. Bioactive coating as a surface modification technique for biocompatible metallic implants: a review. *J. Asian Ceram. Soc.* **2019**, *7*, 397−406.

(4) Asri, R. I. M.; Harun, W. S. W.; Samykano, M.; Lah, N. A. C.; Ghani, S. A. C.; Tarlochan, F.; Raza, M. R. Corrosion and surface modification on biocompatible metals: A review. *Materials Science and Engineering C* **2017**, *77*, 1261−1274.

(5) Niinomi, M. Recent research and development in metallic materials for biomedical, dental and healthcare products applications. *Mater. Sci. Forum* **2007**, *539*−*543*, 193−200.

(6) Aghion, E. Biodegradable metals. *Metals* **2018**, *8*, 804.

(7) Bowen, P. K.; Shearier, E. R.; Zhao, S.; Guillory, R. J.; Zhao, F.; Goldman, J.; Drelich, J. W. Biodegradable Metals for Cardiovascular Stents: From Clinical Concerns to Recent Zn-Alloys. *Adv. Healthc Mater.* **2016**, *5*, 1121−1140.

(8) Hanker, J.; Giammara, B. Biomaterials and biomedical devices. *Science* **1979**, *242* (4880), 885−892.

(9) Agrawal, C. M. Reconstructing the human body using biomaterials. *JOM* **1998**, *50*, 31−35.

(10) Yazdimamaghani, M.; Razavi, M.; Vashaee, D.; Moharamzadeh, K.; Boccaccini, A. R.; Tayebi, L. Porous magnesium-based scaffolds for tissue engineering. *Materials Science and Engineering C* **2017**, *71*, 1253−1266.

(11) Salama, M.; Vaz, M.F.; Colaço, R.; Santos, C.; Carmezim, M., Biodegradable Iron and Porous Iron: Mechanical Properties, Degradation Behaviour, Manufacturing Routes and Biomedical Applications, *J. Funct Biomater 13* (**2022**). DOI: 72.

(12) Wang, X.; Xu, S.; Zhou, S.; Xu, W.; Leary, M.; Choong, P.; Qian, M.; Brandt, M.; Xie, Y. M. Topological design and additive manufacturing of porous metals for bone scaffolds and orthopaedic implants: A review. *Biomaterials* **2016**, *83*, 127−141.

(13) Oriňaková, R.; Gorejová, R.; Králová, Z. O.; Petráková, M.; Oriňak, A. Novel trends and recent progress on preparation methods of biodegradable metallic foams for biomedicine: a review. *J. Mater. Sci.* **2021**, *56*, 13925−13963.

(14) Ma, P. X. Biomimetic materials for tissue engineering. *Adv. Drug Deliv Rev.* **2008**, *60*, 184−198.

(15) Hoang Thi, T. T.; Pilkington, E. H.; Nguyen, D. H.; Lee, J. S.; Park, K. D.; Truong, N. P. The Importance of Poly(ethylene glycol) Alternatives for Overcoming PEG Immunogenicity in Drug Delivery and Bioconjugation. *Polymers* **2020**, *12*, 298.

(16) Tsai, W.B.; Ahmed, I.N., The Impact of Polyethylene Glycol-Modified Chitosan Scaffolds on the Proliferation and Differentiation of Osteoblasts, *Int. J. Biomater 2023* (**2023**). DOI: 1.

(17) Hiromoto, S.; Doi, K. Effect of polyethylene glycol modification on the corrosion behavior of hydroxyapatite-coated AZ31 Mg alloy under tensile deformation. *Corros. Sci.* **2023**, *212*, No. 110931.

(18) Ahirwar, H.; Zhou, Y.; Mahapatra, C.; Ramakrishna, S.; Kumar, P.; Nanda, H.S., Materials for orthopedic bioimplants: Modulating degradation and surface modification using integrated nanomaterials, *Coatings 10* (**2020**). DOI: 264.

(19) Gallo, J.; Holinka, M.; Moucha, C. Antibacterial Surface Treatment for Orthopaedic Implants. *Int. J. Mol. Sci.* **2014**, *15*, 13849−13880.

(20) Roy, A.; Jhunjhunwala, S.; Bayer, E.; Fedorchak, M.; Little, S. R.; Kumta, P. N. Porous calcium phosphate-poly (lactic-co-glycolic) acid composite bone cement: A viable tunable drug delivery system. *Materials Science and Engineering C* **2016**, *59*, 92−101.

(21) Li, Q.; Jiang, G.; Wang, D.; Wang, H.; Ding, L.; He, G. Porous magnesium loaded with gentamicin sulphate and in vitro release behavior. *Materials Science and Engineering C* **2016**, *69*, 154−159.

(22) Aggarwal, D.; Kumar, V.; Sharma, S. Drug-loaded biomaterials for orthopedic applications: A review. *J. Controlled Release* **2022**, *344*, 113−133.

(23) Shahid, A.; Aslam, B.; Muzammil, S.; Aslam, N.; Shahid, M.; Almatroudi, A.; Allemailem, K. S.; Saqalein, M.; Nisar, M. A.; Rasool, M. H.; Khurshid, M. The prospects of antimicrobial coated medical implants. *J. Appl. Biomater. Funct. Mater.* **2021**, *19*, No. 22808000211040304, DOI: 10.1177/22808000211040304.

(24) Channasanon, S.; Udomkusonsri, P.; Chantaweroad, S.; Tesavibul, P.; Tanodekaew, S. Gentamicin Released from Porous Scaffolds Fabricated by Stereolithography. *J. Healthc Eng.* **2017**, *2017*, 1−8.

(25) Chouirfa, H.; Bouloussa, H.; Migonney, V.; Falentin-Daudré, C. Review of titanium surface modification techniques and coatings for antibacterial applications. *Acta Biomater* **2019**, *83*, 37−54.

(26) Nichol, T.; Callaghan, J.; Townsend, R.; Stockley, I.; Hatton, P. V.; Le Maitre, C.; Smith, T. J.; Akid, R. The antimicrobial activity and biocompatibility of a controlled gentamicin-releasing single-layer sol-gel coating on hydroxyapatite-coated titanium. *Bone Joint J.* **2021**, *103-B*, 522−529.

(27) Kan, Y. C.; Guo, R.; Xu, Y.; Han, L. Y.; Bu, W. H.; Han, L. X.; Chu, J. J. Investigating the in vitro antibacterial efficacy of composite bone cement incorporating natural product-based monomers and gentamicin. *J. Orthop. Surg. Res.* **2024**, *19*, 169 DOI: 10.1186/s13018-024-04646-7.

(28) Antoci, V.; Adams, C. S.; Hickok, N. J.; Shapiro, I. M.; Parvizi, J. Antibiotics for local delivery systems cause skeletal cell toxicity in vitro. *Clin Orthop Relat Res.* **2007**, *462*, 200−206.

(29) Xie, Z.; Cui, X.; Zhao, C.; Huang, W.; Wang, J.; Zhang, C. Gentamicin-loaded borate bioactive glass eradicates osteomyelitis due to Escherichia coli in a rabbit model. *Antimicrob. Agents Chemother.* **2013**, *57*, 3293−3298.

(30) Schneider, C. A.; Rasband, W. S.; Eliceiri, K. W. NIH Image to ImageJ: 25 years of image analysis. *Nat. Methods* **2012**, *9*, 671−675.

(31) Standard Test Method for Conducting Potentiodynamic Polarization Resistance Measurements, 2009. www.astm.org,.
(32) ASTM G31-72. *ASTM G31: Standard Practice for Laboratory Immersion Corrosion Testing of Metals*, 2004.
(33) ISO-10993-5. *Biological evaluation of medical devices—part 5 tests for cytotoxicity: in vitro methods*; ANSI/AAMI: Arlington, 2009; pp 1−34.
(34) Fu, X.; Kong, W.; Zhang, Y.; Jiang, L.; Wang, J.; Lei, J. Novel solid-solid phase change materials with biodegradable trihydroxy surfactants for thermal energy storage. *RSC Adv.* **2015**, *5*, 68881−68889.
(35) Batul, R.; Bhave, M.; Mahon, P. J.; Yu, A. Polydopamine nanosphere with in-situ loaded gentamicin and its antimicrobial activity. *Molecules* **2020**, *25*, 2090.
(36) Francis, L.; Meng, D.; Knowles, J.; Keshavarz, T.; Boccaccini, A. R.; Roy, I. Controlled delivery of gentamicin using poly(3-hydroxybutyrate) microspheres. *Int. J. Mol. Sci.* **2011**, *12*, 4294−4314.
(37) Naraharisetti, P. K.; Ning Lew, M. D.; Fu, Y. C.; Lee, D. J.; Wang, C. H. Gentamicin-loaded discs and microspheres and their modifications: Characterization and in vitro release. *J. Controlled Release* **2005**, *102*, 345−359.
(38) Kawai, F. Biodegradation of Polyethers (Polyethylene Glycol, Polypropylene Glycol, Polytetramethylene glycol, and Others). In Matsumura, S.; Steinbüchel, A., Eds.; *Biopolymers Online*; Wiley, 2001.
(39) Haverová, L.; Oriňaková, R.; Oriňak, A.; Gorejová, R.; Baláž, M.; Vanýsek, P.; Kupková, M.; Hrubovčáková, M.; Mudroň, P.; Radoňák, J.; Králová, Z. O.; Turoňová, A. M. An in vitro corrosion study of open cell Iron structures with PEG coating for bone replacement applications. *Metals* **2018**, *8*, 499.
(40) Karahan, H. Effect of current density on the corrosion protection performance of polyaniline coated AISI 4140 steel. *Transactions of the Institute of Metal Finishing* **2019**, *97*, 48−52.
(41) Oriňaková, R.; Gorejová, R.; Országová Králová, Z.; Haverová, L.; Oriňak, A.; Maskal'ová, I.; Kupková, M.; Džupon, M.; Baláž, M.; Hrubovčáková, M.; Sopčák, T.; Zubrik, A.; Oriňak, M. Evaluation of mechanical properties and hemocompatibility of open cell iron foams with polyethylene glycol coating. *Appl. Surf. Sci.* **2020**, *505*, No. 144634.
(42) Oriňaková, R.; Gorejová, R.; Petráková, M.; Králová, Z. O.; Oriňak, A.; Kupková, M.; Hrubovčáková, M.; Podobová, M.; Baláž, M.; Smith, R. M. Degradation performance of open-cell biomaterials from phosphated carbonyl iron powder with PEG coating. *Materials* **2020**, *13*, 4134.
(43) Fan, L.; Sun, W.; Zou, Y.; Qian Xu, Q.; Zeng, R. C.; Tian, J. Enhanced corrosion resistance, antibacterial activity and biocompatibility of gentamicin-montmorillonite coating on Mg alloy-in vitro and in vivo studies. *J. Mater. Sci. Technol.* **2022**, *111*, 167−180.
(44) Zhang, Z. Q.; Wang, L.; Zeng, M. Q.; Zeng, R. C.; Lin, C. G.; Wang, Z. L.; Chen, D. C.; Zhang, Q. Corrosion resistance and superhydrophobicity of one-step polypropylene coating on anodized AZ31 Mg alloy. *Journal of Magnesium and Alloys* **2021**, *9*, 1443−1457.
(45) Yang, Y.; Fan, M.; Zhao, F. Degradation behavior, cytotoxicity, hemolysis of partially unzipped carbon nanotubes/zinc composites as potential biodegradable bone implants. *Biomedical Materials* **2023**, *18*, No. 045016.
(46) Zeller-Plumhoff, B.; Helmholz, H.; Feyerabend, F.; Dose, T.; Wilde, F.; Hipp, A.; Beckmann, F.; Willumeit-Römer, R.; Hammel, J. U. Technical note on the determination of degradation rates of biodegradable magnesium implants. *Materials and Corrosion* **2023**, *74*, 1116−1119.
(47) Ranjan, A.; Pothayee, N.; Seleem, M. N.; Tyler, R. D.; Brenseke, B.; Sriranganathan, N.; Riffle, J. S.; Kasimanickam, R. Antibacterial efficacy of core-shell nanostructures encapsulating gentamicin against an in vivo intracellular Salmonella model. *Int. J. Nanomedicine* **2009**, *4*, 289−297.
(48) Katsikogianni, M.; Missirlis, Y. F.; Harris, L.; Douglas, J. Concise review of mechanisms of bacterial adhesion to biomaterials and of techniques used in estimating bacteria-material interactions. *Eur. Cell Mater.* **2004**, *8*, 37−57.
(49) Fan, L.; Sun, W.; Zou, Y.; Qian Xu, Q.; Zeng, R. C.; Tian, J. Enhanced corrosion resistance, antibacterial activity and biocompatibility of gentamicin-montmorillonite coating on Mg alloy-in vitro and in vivo studies. *J. Mater. Sci. Technol.* **2022**, *111*, 167−180.

https://doi.org/10.1021/acsomega.4c01002
ACS Omega 2024, 9, 27113−27126